Natural Convection in an Enclosure Heated from Below with a Conductive Horizontal Partition

Heiu-Jou Shaw,* Cha'o-Kuang Chen,† and Jiin-Yuh Jang‡
National Cheng-Kung University, Tainan, Taiwan, Republic of China

This paper investigates the phenomenon of natural convection in an enclosure heated from below, fitted with a completely horizontal conductive partition. The horizontal partition is parallel to the two horizontal isothermal enclosure walls, which are maintained at different temperatures, while the vertical walls of the enclosure are adiabatic. The governing equations for stream function, vorticity, and energy are solved with the aid of the cubic spline collocation method. Parametric studies of the effects of the partition on the fluid flow and temperature fields in the enclosure have been performed. Numerical results indicate that the effects of the conductivity ratio of the partition and the aspect ratio of the enclosure on the heat-transfer rate are not significant. However, the location of the partition affects the fluid flow and heat-transfer rate profoundly. Numerical results are also compared with the results obtained from a flow visualization experiment. The streamline distribution obtained from numerical result is shown to be in good agreement with the experimental results.

Nomenclature

A = L/H = geometric aspect ratio
g = gravitational acceleration
H = enclosure height
H_1, H_2 = upper and lower subenclosure heights, respectively
k, k_w = thermal conductivity of the fluid and solid wall, respectively
KR = thermal conductivity ratio (k_w/k)
L = enclosure length
m, n = number of vertical and horizontal grid lines, respectively
Nu = Nusselt number
Nu^* = modified Nusselt number defined by Ref. 10
Pr = Prandtl number
Q = heat transfer across enclosure
Ra = Rayleigh number based on H
t, τ = dimensional and dimensionless time, respectively
T = temperature
T_H = warm end temperature
T_L = cold end temperature
T_{LP}, T_{UP} = average temperatures at lower and upper surfaces of the partition, respectively
W = width of the horizontal wall
ΔT = temperature difference between the hot and cold wall
u, U = dimensional and dimensionless horizontal velocity, respectively
v, V = dimensional and dimensionless vertical velocity, respectively
x, X = dimensional and dimensionless horizontal coordinates, respectively
y, Y = dimensional and dimensionless vertical coordinates, respectively
α, α_w = thermal diffusivity of the fluid and the partition, respectively
β, β_w = coefficients of thermal expansion of the fluid and partition, respectively
μ = viscosity
ν = kinematic viscosity, $= \mu/\rho$
ρ, ρ_w = density of the fluid and partition, respectively
ψ, Ψ = dimensional and dimensionless stream function, respectively
θ = dimensionless temperature of the fluid
θ_w = dimensionless temperature of the partition
ω, Ω = dimensional and dimensionless vorticity, respectively

Received April 22, 1987; revision received Oct. 2, 1987.

*Lecturer, Department of Naval Architecture and Marine Engineering.
†Professor, Department of Mechanical Engineering.
‡Associate Professor, Department of Mechanical Engineering.

Introduction

THE problem of buoyancy-driven flow in an enclosure has many practical applications. Well-known examples are the energy conservation in building enclosures, solar collection spaces, and thermal-energy storage systems.

There are several experimental and numerical studies on natural convection heat transfer in simple enclosures heated from the side.[1,2] However, the consideration of natural air motion through a completely separated partition in an enclosure has a relatively short history. Among the earlier theoretical contributions, only a few papers are concerned with this problem. Koutsoheras and Charters[3] carried out numerical studies for the rectangular enclosure that take account of two-dimensional conduction in the left vertical wall. In the other papers considering the conjugate problem,[4-6] heat-transfer measurements and flow visualization investigations were conducted for different Rayleigh numbers and geometrical parameters. In addition, the phenomenon of natural convection in an enclosure heated from below has many engineering applications and has been discussed in numerous studies.[7,8] Recently, Catton and Lienhard[9] and Lienhard and Catton[10] used a Galerkin approximation method and Landau method to analyze the natural convective heat transfer across a two-fluid-layer region with a thermal barrier. In those studies,[9,10] the two-fluid layer is restricted to the infinite domain.

The purpose of this paper is to investigate numerically the two-dimensional, laminar natural convection flow, in a rectangular enclosure heated from below, fitted with a completely separated horizontal partition. Parametric studies of the effects of the partition on fluid flow and temperature fields in the enclosure have been performed, as well as studies to determine the effect on the flow of various locations and widths, and on the material of horizontal partition for different Rayleigh num-

bers (10^3–10^6). Furthermore, flow visualization experiments are carried out to verify the theoretical predictions.

Numerical computation is accomplished with the aid of the cubic spline collocation method. This numerical scheme has been successfully applied to solve the partial differential equations in fluid mechanics by Rubin and co-workers[11–13] and others.[14]

Mathematical Formulation

The geometry and coordinate system of the problem are given in Fig. 1. A Cartesian coordinate system is adopted, with the y axis in the direction opposite to the gravity vector and the origin placed at the left bottom corner of the cavity. The two-dimensional rectangular enclosure is fitted with a completely separated internal partition. The horizontal walls of the enclosure are kept isothermal at different temperatures, whereas the vertical walls are insulated. Within the internal partition in the enclosure, conduction is two-dimensional. All fluid properties are assumed constant, and the fluid is considered to be incompressible except for the buoyancy term, which is computed using the Boussinesq-type equation of state. Viscous dissipation and compression work are neglected in the energy equation, as are the radiation effects.

The vorticity and stream function are used to eliminate pressure as a variable and to eliminate the need for the direct inclusion of the continuity equation in the investigation. The resulting governing equations for the fluids in the two subenclosures are

$$\frac{\partial\theta}{\partial\tau}+U\frac{\partial\theta}{\partial X}+V\frac{\partial\theta}{\partial Y}=\nabla^2\theta \tag{1}$$

$$\frac{\partial\Omega}{\partial\tau}+\frac{\partial(U\Omega)}{\partial X}+\frac{\partial(V\Omega)}{\partial Y}=Ra\,Pr\frac{\partial\theta}{\partial X}+Pr\,\nabla^2\Omega \tag{2}$$

$$\Omega=-\nabla^2\Psi \tag{3}$$

where

$$U=\frac{\partial\Psi}{\partial Y},\qquad V=-\frac{\partial\Psi}{\partial X}$$

The energy equation for the internal conductive partition is

$$\frac{\partial\theta_w}{\partial\tau}=KR\left[\frac{\partial^2\theta_w}{\partial X^2}+\frac{\partial^2\theta_w}{\partial Y^2}\right] \tag{4}$$

The dimensionless variables $X=x/L$, $Y=y/L$, $\tau=t/(L^2/\alpha)$, $U=u/(\alpha/L)$, $\Omega=\omega/(\alpha/L^2)$, $\Psi=\psi/\alpha$, $\theta=(T-T_L)/(T_H-T_L)$, and $\theta_w=(T_w-T_L)/(T_H-T_L)$ represent the dimensionless coordinates, time, velocity, vorticity, stream function, fluid temperature, and solid temperature, respectively.

The boundary conditions are:

$$\begin{aligned}
&Y=0, \quad \theta=1, \quad U=V=0\\
&Y=1, \quad \theta=0, \quad U=V=0\\
&X=0,1 \quad \frac{\partial\theta}{\partial X}=0, \quad U=V=0\\
&Y=H_2/L,\ (H_2+W)/L, \quad KR\left[\frac{\partial\theta_w}{\partial Y}\right]_{\text{solid}}=\left[\frac{\partial\theta}{\partial Y}\right]_{\text{fluid}} \quad U=V=0
\end{aligned} \tag{5}$$

In the preceding equations, three governing parameters appear: the Prandtl number, $Pr=\nu/\alpha$; the Rayleigh number, $Ra=\beta gL^3(T_H-T_L)/\nu\alpha$; and the location of partition, H_2/L. In this study, the Prandtl number is assigned a value of 1.0, the Rayleigh number takes on values in the range of 10^3–10^6, and the partition height H_2/L is assigned the values of 0.1, 0.2, 0.3, 0.4, and 0.5.

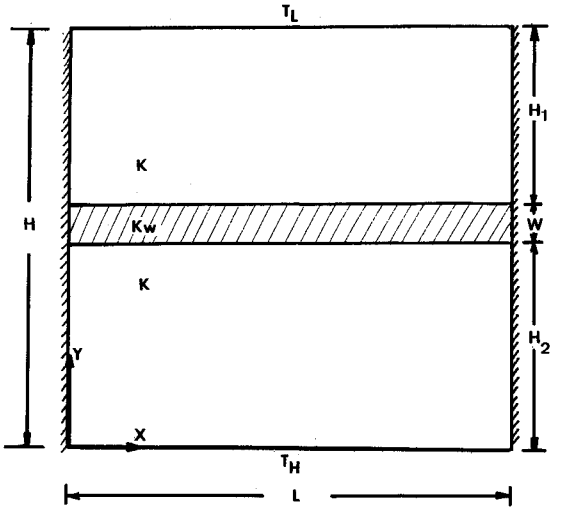

Fig. 1 The physical model.

Since the vertical walls are adiabatic, heat transfer occurs only in the vertical direction. The overall Nusselt number for the net heat transfer in the vertical direction is defined as

$$Nu=\frac{Q}{k(T_H-T_C)}=\int_0^1\left[\frac{\partial T}{\partial Y}\right]_{Y=0,1}dX \tag{6}$$

or[10]

$$Nu^*=\frac{k_w[(T_{LP}-T_{UP})/w]}{[k(T_H-T_C)/H_2]\{1+H_1/H_2+[w/(H_1H_2)]k/k_w(1+H_1/H_2)\}-1} \tag{7}$$

The numerical integration of Eq. (6) or (7) was performed after the steady-state temperature field was obtained.

Numerical Procedure

The coupled equations (1–4), with the associated boundary conditions, provide a complete mathematical specification of the problem. The equations are solved by the cubic spline collocation method.[11–14]

The main advantages of using the cubic spline procedure are:

1) The governing matrix system is always tridiagonal so that well-developed and highly efficient inversion algorithms, such as the Thomas algorithm, are applicable.

2) It has been demonstrated that the spatial accuracy of the spline approximation for the first derivatives is fourth-order accurate for a uniform mesh and third-order accurate for a nonuniform mesh. The second derivatives are second-order accurate for uniform as well as nonuniform grids.

3) Derivative boundary conditions can be directly incorporated into the inversion procedure.

Solutions are obtained by an iterative SADI (spline alternating direction implicit) procedure. The SADI system representing the governing equations follows.

Stream-Function Equation

Step 1:

$$\Psi_{ij}^{n+1,s+\frac{1}{2}}=\Psi_{ij}^{n+1,s}+\frac{\Delta\sigma}{2}\{(\Psi_{YY})_{ij}^{n+1,s+\frac{1}{2}}+(\Psi_{XX})_{ij}^{n+1,s}+\Omega_{ij}^{n+1}\} \tag{8}$$

Step 2:

$$\Psi_{ij}^{n+1,s+1}=\Psi_{ij}^{n+1,s+\frac{1}{2}}+\frac{\Delta\sigma}{2}\{(\Psi_{YY})_{ij}^{n+1,s+\frac{1}{2}}+(\Psi_{XX})_{ij}^{n+1,s+1}+\Omega_{ij}^{n+1}\} \tag{9}$$

where $\Delta\sigma$ is a fictitious time step and $\sigma = s\Delta\sigma$. Solutions for Eqs. (8) and (9) are the steady-state limit ($\tau \to \infty$) of Eq. (3).

Vorticity Equation

Step 1:

$$\Omega_{ij}^{n+\frac{1}{2}} = \Omega_{ij}^{n} + \frac{\Delta\tau}{2}\{-(\Psi_Y)_{ij}^{n}(\Omega_X)_{ij}^{n} + (\Psi_X)_{ij}^{n}(\Omega_X)_{ij}^{n+\frac{1}{2}} + Pr(\Omega_{XX})_{ij}^{n} + Pr(\Omega_{YY})_{ij}^{n+\frac{1}{2}} + Ra\,Pr(\theta_X)_{ij}^{n}\} \quad (10)$$

Step 2:

$$\Omega_{ij}^{n+1} = \Omega_{ij}^{n+\frac{1}{2}} + \frac{\Delta\tau}{2}\{-(\Psi_Y)_{ij}^{n}(\Omega_X)_{ij}^{n+1} + (\Psi_X)_{ij}^{n}(\Omega_Y)_{ij}^{n+\frac{1}{2}} + Pr(\Omega_{XX})_{ij}^{n+1} + Pr(\Omega_{YY})_{ij}^{n+\frac{1}{2}} + Ra\,Pr(\theta_X)_{ij}^{n}\} \quad (11)$$

Energy Equation

Step 1:

$$\theta_{ij}^{n+\frac{1}{2}} = \theta_{ij}^{n} + \frac{\Delta\tau}{2}\{-(\Psi_Y)_{ij}^{n}(\theta_X)_{ij}^{n} + (\Psi_X)_{ij}^{n}(\theta_Y)_{ij}^{n+\frac{1}{2}} + (\theta_{XX})_{ij}^{n} + (\theta_{YY})_{ij}^{n+\frac{1}{2}}\} \quad (12)$$

Step 2:

$$\theta_{ij}^{n+1} = \theta_{ij}^{n+\frac{1}{2}} + \frac{\Delta\tau}{2}\{-(\Psi_Y)_{ij}^{n}(\theta_X)_{ij}^{n+1} + (\Psi_X)_{ij}^{n}(\theta_Y)_{ij}^{n+\frac{1}{2}} + (\theta_{XX})_{ij}^{n+1} + (\theta_{YY})_{ij}^{n+\frac{1}{2}}\} \quad (13)$$

After some rearrangement, Eqs. (8–13) may be written in the following form [10]:

$$\phi_{ij}^{p+\frac{1}{2}} = F_{ij}^{p} + G_{ij}\,1_{\phi_{ij}}^{p+\frac{1}{2}} + S_{ij} + L_{\phi_{ij}}^{p+\frac{1}{2}} \quad (14)$$

$$\phi_{ij}^{p+1} = F_{ij}^{p+\frac{1}{2}} + G_{ij}\,m_{\phi_{ij}}^{p+1} + S_{ij}\,M_{\phi_{ij}}^{p+1} \quad (15)$$

where ϕ represent the functions Ψ, Ω, and θ.

In this relation between the function and its first two derivatives, the quantities F_{ij}, G_{ij}, S_{ij} are known coefficients evaluated at previous time steps. It should be noted that Eqs. (14) and (15) are very general and do not depend on the method for spatial integration.

Equations (14) and (15), when combined with the cubic spline relations described in Ref. 14, may be written in tridiagonal form as

$$a_{i,j-1}\,\Phi_{ij}^{n+1} + b_{ij}\,\Phi_{ij}^{n+1} + c_{i,j+1}\,\Phi_{ij}^{n+1} = d_{ij} \quad (16)$$

where Φ represent the function (Ψ, Ω, θ) or its first two derivatives. Equation (16) is easily solved by using the Thomas algorithm. A double iterative procedure is described as follows:

1) Initially, the stream function is assumed zero everywhere.

2) The temperature distribution is obtained with the SADI technique as presented in Eqs. (12) and (13). At the initial state, the solution describes the temperature distribution for the pure conduction case.

3) The temperature distribution and the associated stream-function field are then substituted into the vorticity equation, from which a distribution for vorticity is obtained. The boundary conditions are determined by

$$\Omega_{i,0} = \left.\frac{\partial^2\Psi}{\partial x^2}\right|_x + \left.\frac{\partial^2\Psi}{\partial y^2}\right|_{y=0} \quad (17)$$

$$\Omega_{0,j} = \left.\frac{\partial^2\Psi}{\partial x^2}\right|_{x=0} + \left.\frac{\partial^2\Psi}{\partial y^2}\right|_y \quad (18)$$

4) The stream-function field is calculated from the obtained vorticity by using a fictitious unsteady-state term. The solution for the stream function was ascertained by insuring that the following residual-error criterion is satisfied:

$$\left|\frac{\Psi_{ij}^{s} - \Psi_{ij}^{s-1}}{\Psi_{\max}^{s}}\right| < 10^{-4} \quad (19)$$

where superscripts s and $(s-1)$ denote the current and the previous iterations, respectively.

5) If only the steady-state solution is required, the calculation proceeds to the next time step by returning to step 2 with $n \to n+1$. The iteration process was employed until the maximum relative change in temperature and flowfields satisfies the following criterion:

$$\left|\frac{\Phi_{ij}^{z} - \Phi_{ij}^{z-1}}{\Phi_{\max}^{z}}\right| < 10^{-4} \quad (20)$$

and by computing a heat balance for the enclosure

$$\left|\frac{Nu^{z} - Nu^{z-1}}{Nu^{z}}\right| < 0.005 \quad (21)$$

In the preceding criterion, Φ refers to Ψ, θ, and Ω and z denotes the number of false time steps.

On the other hand, if an accurate transient solution is required, the iterative calculations proceed from step 2 to step 4. This process continues until convergence. The steay-state condition is also reached by using the criterion defined earlier. Although accurate transient computations have been performed in a number of cases, only the steady-state results are presented in this paper.

The convergence behavior of the numerical method is checked by running with different mesh sizes. The overall Nusselt number was used to develop an understanding of how many grid points are necessary for accurate numerical simulations. It was found that 25 × 25 grid points were sufficient to provide accurate results (Fig. 2).

Experimental Procedure

The experiment of flow visualization is performed in order to examine the assumptions of the numerical model of the problem considered in this paper. The partitioned enclosure used in this experiment is of aspect ratio $A = 1$ and 3. The schematic diagram of the flow visualization experiment is shown in Fig. 3. The isothermal condition on each of the surfaces is maintained

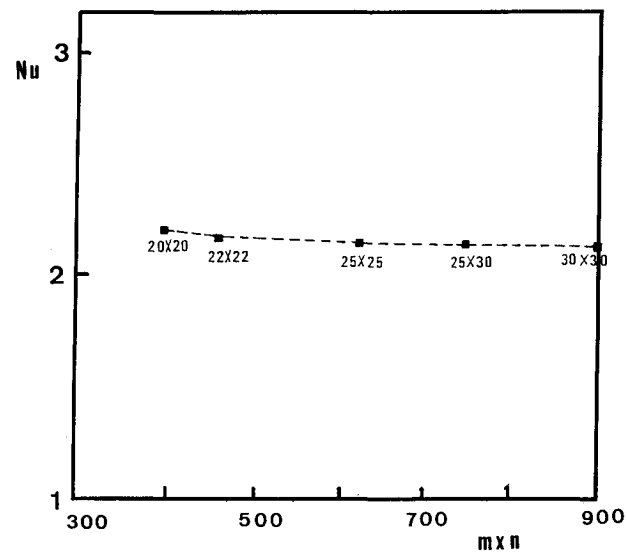

Fig. 2 Influence of mesh size on the accuracy of overall heat-transfer rate estimates.

by a plate heat exchanger. On the back side of the copper test surface, water, as the exchanger fluid, flows back and forth over the length of the test surface. The water circulated in the heat exchanger is driven by a constant-temperature circulator. Surface temperatures are measured using copper-constantan thermocouples embedded in the copper plate. In order to observe flow patterns, cigarette smoke was injected into the twin air layers in the test section. A flat narrow slit of light illuminated the smoke particles against a dark background. A Nikon EM camera was used to record this investigation.

Results and Discussion

The numerical procedure described was programmed in Turbo Pascal language and performed on an IBM personal computer (PC/XT).

Results presented will include the flow pattern, dimensionless streamline, isotherm contour plots, and the average heat flux ratios along the boundaries of the enclosure.

Effect of the Rayleigh Number

The effects of the Rayleigh number on the Nusselt number are illustrated in Fig. 4. Figure 4a shows the numerical results for $A = 1$ and $A = 10$. The two numerical results are in good agreement with the result obtained by Lienhard and Catton (KR = 1).[10] Since the heat-transfer phenomenon obtained by Lienhard and Catton is in the infinite fluid region, our numerical result is in better agreement for large aspect ratios ($A = 10$). Figure 4b presents the effects of the Rayleigh number on the Nusselt number for the conductivity ratio (KR) of 10. It can be seen that an increase in Rayleigh number will significantly increase the Nusselt number. The streamlines and isotherms for a square enclosure heated from below with separated horizontal partitions for $Ra = 10^4$ and 10^5 are presented in Fig. 5. Evidently, each two convective cells are separated by a horizontal partition, and the isotherms are distorted as described by the flow pattern and temperature distribution in these figures.

Effect of the Ratio of Conductivity of Partition

The Nusselt number is plotted against the ratio of conductivity (KR) of partition in Fig. 6. The Nusselt number is increased as the KR increases from 1 to 10. When the value of KR is increased from 10 to 100, however, the Nusselt number decreases slightly. Therefore, the Nusselt number reaches maximum value at $KR = 10$. This behavior is explained in Fig. 7, which demonstrates the temperature distribution of the horizontal partition for various values of the ratio of conductivity (KR). As the KR decreases, the Y-direction temperature gradient becomes larger. When the value of KR becomes larger, temperature distribution is more uniform, but the temperature gradient becomes smaller. Although the Y-direction temperature gradient becomes smaller, the Nusselt number increases. This situation is due to the increase in the conductivity of the partition inside two flow regions. If, however, the value of KR is increased from 10 to 100, the temperature gradient becomes very small although the conductivity of the partition is increased. A slight decrease in Nusselt number results. Figure 8 presents the effect of the ratio of conductivity of fluid and partition on the square enclosure. The streamlines and isotherms are plotted for $KR = 5$ and 100, respectively. The convective phenomenon is separated between the partition and the boundary of enclosure, as described in the flow and isotherm pattern shown in Fig. 8.

Effect of Different Locations of the Horizontal Partition

Numerical results of fluid velocity and temperature field are presented using velocity vectors and isotherms in Fig. 9. The computational results will be affected by different locations of horizontal partitions. The velocity vectors and isotherms are plotted for $H_2/L = 0.1$, 0.3, and 0.4, respectively, in the case of $KR = 10$ and $Ra = 10^5$. The isotherms are distorted as the location of the partition (H_2/L) is varied. Evidently, two convective cells are formed below and above the horizontal partition when it is placed at $H_2/L = 0.4$.

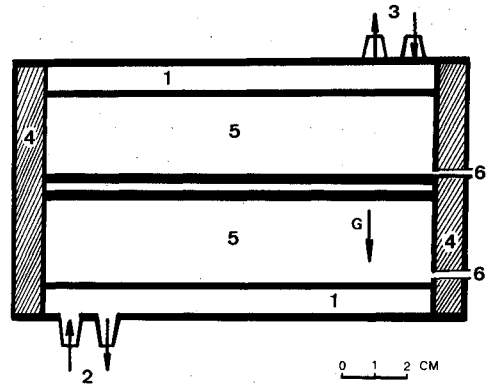

1) Copper plate
2) High-temperature water flow
3) Low-temperature water flow
4) Insulator
5) Air
6) Needle hole
7) Partition

Fig. 3 Experimental model for flow visualization.

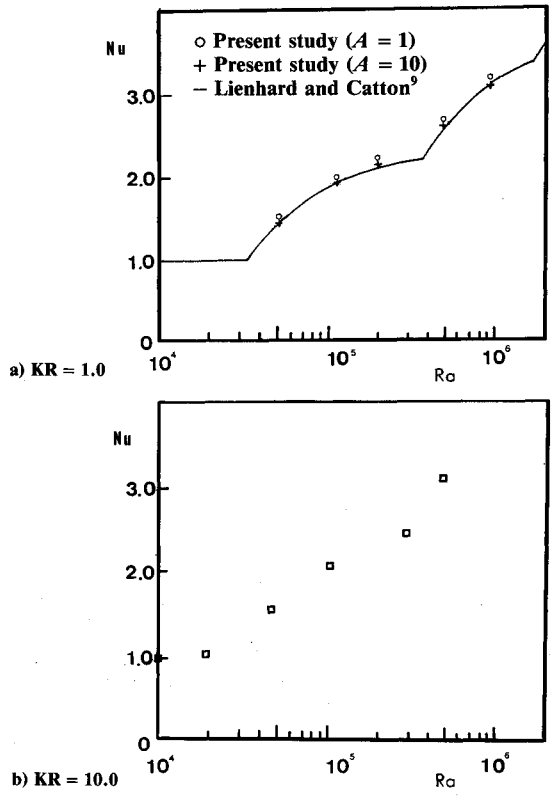

Fig. 4 Effects of Rayleigh number on Nusselt number ($Ra = 10^5$, $A = 1.1$, $H_2/L = 0.5$, $W/L = 0.1$).

Figure 10 shows how the location of the partition (H_2/L) affects the Nusselt number. It is clear that the Nusselt number is decreased sharply as the H_2/L is increased from 0 to 0.3, then increased as H_2/L is in the range 0.3–0.5. However, as H_2/L is in the range 0.5–0.9, the Nusselt number is again increased significantly. The figure is symmetric about $H_2/L = 0.5$. As can be seen from the Fig. 10, the Nusselt number attains the highest value at $H_2/L = 0.1$ and the lowest value at $H_2/L = 0.3$. At $H_2/L = 0.1$, the fluid in the small subenclosure has almost no convective flow motion, so that the temperature distribution is in a state of conduction. The convective phenomena exist only inside the large subenclosure. When H_2/L reaches the value of 0.3, the heat-transfer phenomenon in the smaller subenclosure

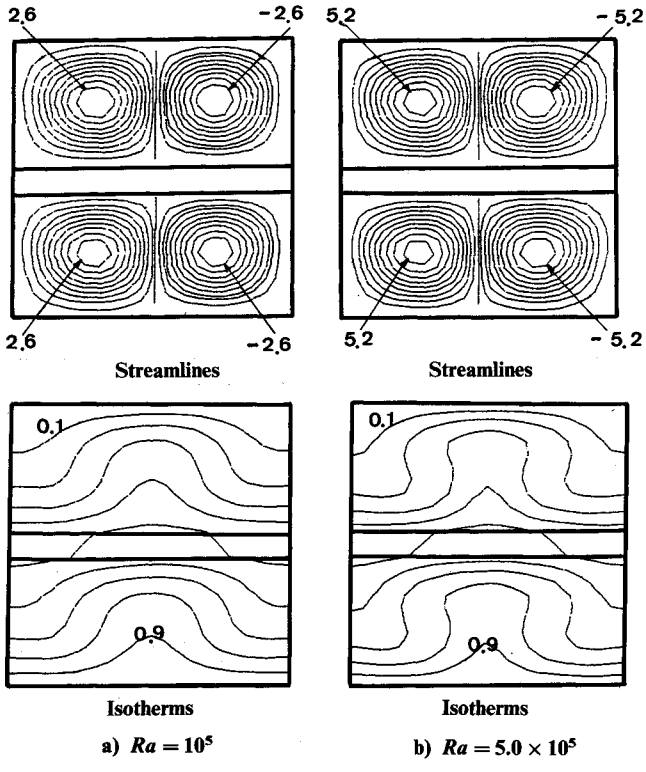

Fig. 5 Isotherms and streamlines of the flowfield for $A = 1$, $H_2/L = 0.5$, $W/L = 0.1$, $KR = 10$, $Ra = 10^5$, and 5.0×10^5 ($\Delta\Psi = 0.3$, $\Delta\theta = 0.1$).

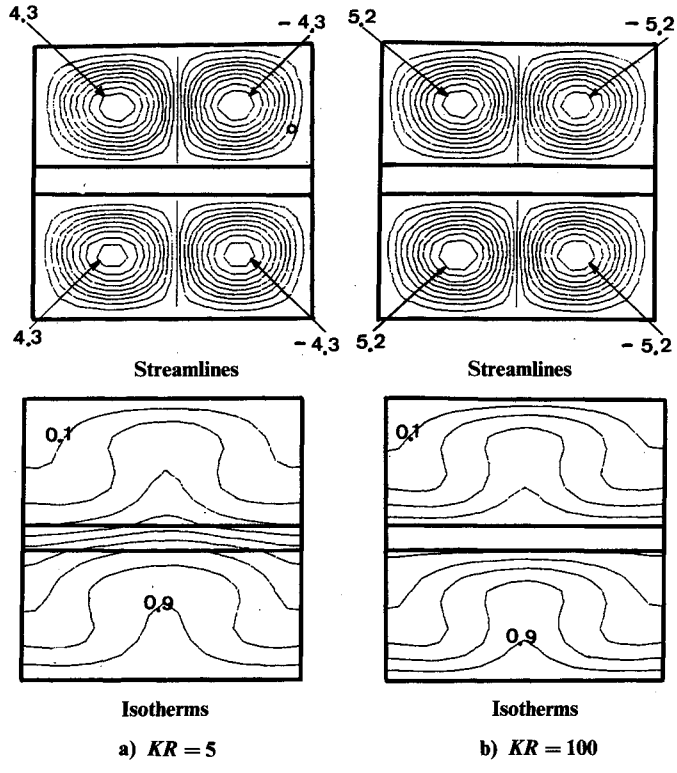

Fig. 7 Isotherms and streamlines of the flowfield for $Ra = 10^5$. $A = 1.1$, $H_2/L = 0.1$, $KR = 5$ and 100 ($\Delta\Psi = 0.3$, $\Delta\theta = 0.1$).

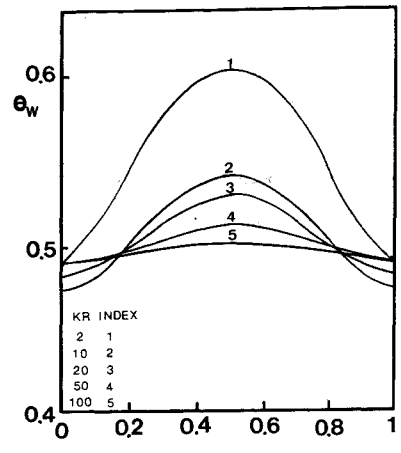

Fig. 6 Temperature distribution of lower surface of the partition for various KR ($Ra = 10^5$, $H_2/L = 0.5$, $W/L = 0.1$).

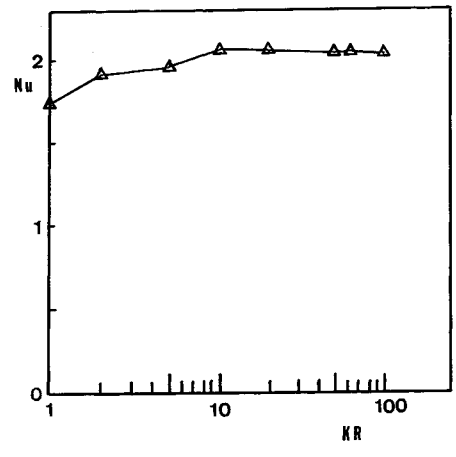

Fig. 8 Effect of KR on Nusselt number ($Ra = 10^5$, $A = 1.1$, $H_2/L = 0.5$, $W/L = 0.1$).

is also dominated by conduction. Relatively, the convective region inside the whole enclosure will become smaller. This will significantly decrease the Nusselt number. However, as the value of H_2/L is increased again to 0.5 (Fig. 5a), the Nusselt number is increased, owing to the existence of the Bénard cell, and it will increase the convective flow in the two subenclosures. Consequently, the Nusselt number is decreased again until the H_2/L reaches the value of 0.7 and the Bénard cell will increase at the center.

Effect of the Thickness of Partition

The Nusselt number is affected by the variation of the width of the horizontal wall (W/L) inside an enclosure. Figure 11 illustrates that the Nusselt number is decreased slightly as the width of the enclosure is increased.

Effect of the Geometric Aspect Ratio

It is important to examine the effect of the geometric aspect ratio on the partitioned enclosure. A series of numerical experiments illustrating this effect were conducted by varying the length for $L = 2H$ and $L = 3H$. The streamlines and isotherms are demonstrated in Fig. 12. The results show that as the aspect ratio increases at constant Ra, the number of cells increases discretely. But the effect of the aspect ratio of the enclosure on the heat-transfer rate is not significant, as shown in Fig. 4a.

Flow Visualization

Figures 13 and 14 present photographs of streamline distribution in the twin air layer for aspect ratio $A = 1$ and 2, respectively, for the case of $Ra = 10^5$. The partition of the enclosure is made of brass. Figure 13 reveals the phenomena of natural

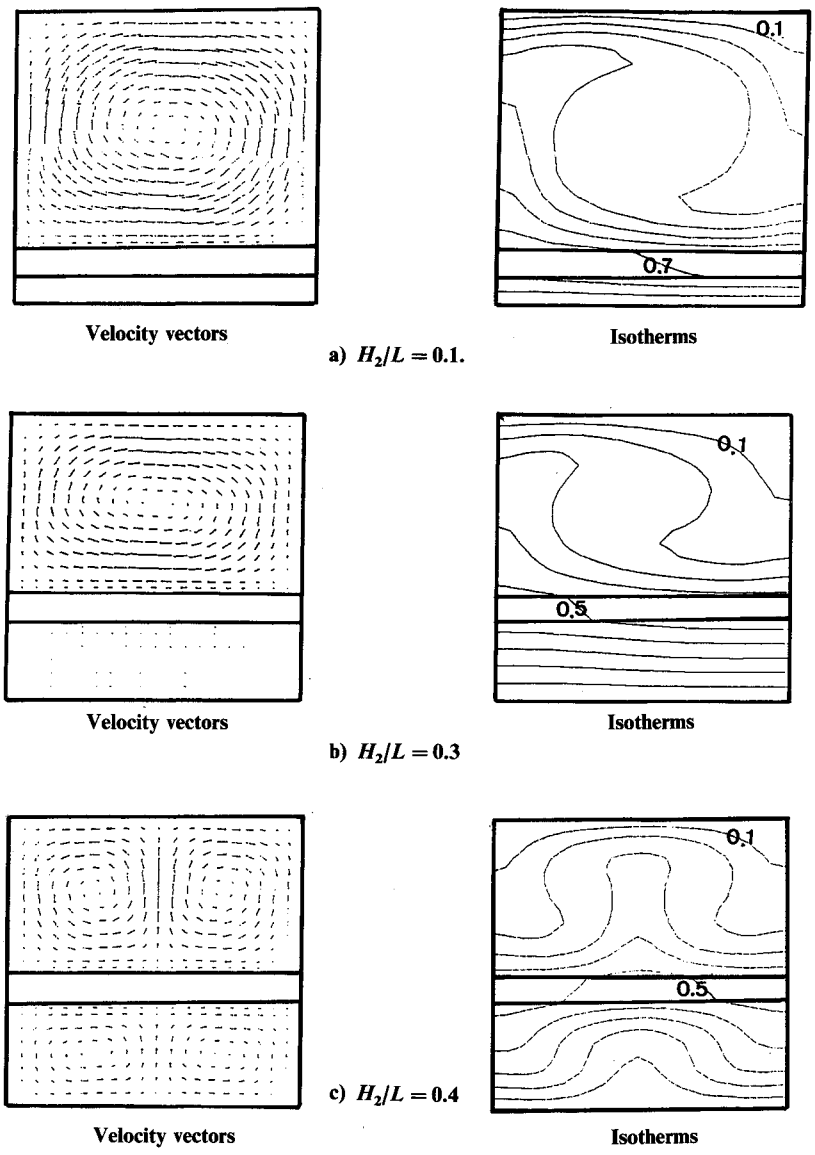

Fig. 9 Effect of different locations of horizontal partition on velocity vectors and isotherms ($Ra = 10^5$, $A = 1.1$, $W/L = 0.1$, $KR = 10$, $\Delta\theta = 0.1$).

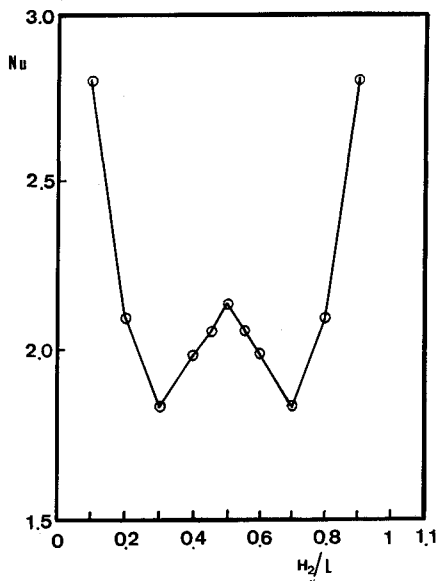

Fig. 10 Effect of different locations of horizontal partition (H_2/L) on Nusselt number ($Ra = 10^5$, $A = 1.1$, $W/L = 0.1$, $KR = 10$).

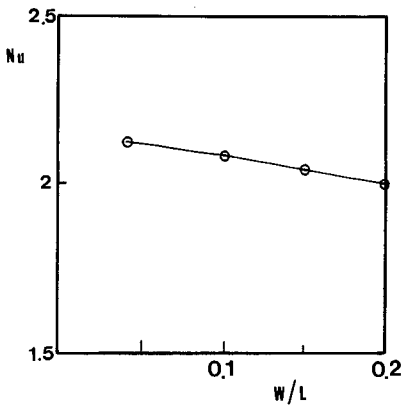

Fig. 11 Effect of thickness of partition (W/L) on Nusselt number ($Ra = 10^5$, $A = 1.1$, $KR = 10$).

convection, with two cells inside the upper and lower subenclosure, respectively, for aspect ratio $A = 1$. This behavior is caused by the heating of the enclosure at the bottom. However, Fig. 14 shows that four cells exist inside each of these two

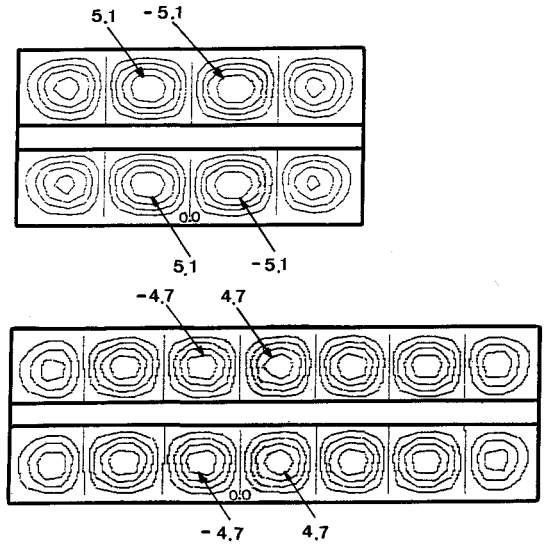

a) Streamlines for $L = 2H$ and $L = 3H$

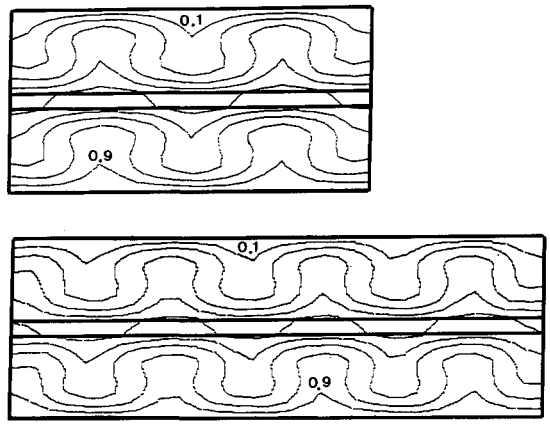

b) Isotherms for $L = 2H$ and $L = 3H$

Fig. 12 Effect of geometric aspect ratios of enclosure on streamlines and isotherms ($Ra = 10^5$, $KR = 10$, $\Delta\Psi = 1.3$, $\Delta\theta = 0.1$).

subenclosures for $A = 2$. Those results are seen to be in good agreement with the numerical results as shown in Figs. 8a and 12b. Hence, the numerical model is proved to be reliable.

Conclusion

Natural convection heated from below in an enclosure with a conductive partition has been analyzed numerically. The study focused on the effect of the partition on the natural convection phenomenon in an enclosure. The numerical results indicate that the effects of conductivity of the partition and of the aspect ratio of the enclosure on the heat-transfer rate of the partitioned enclosure are not significant. However, the locations of the partition affects the heat-transfer rate profoundly. Increase in the partition's thickness decreases the heat-transfer rate. The numerical method is proved to be reliable by a flow visualization experiment.

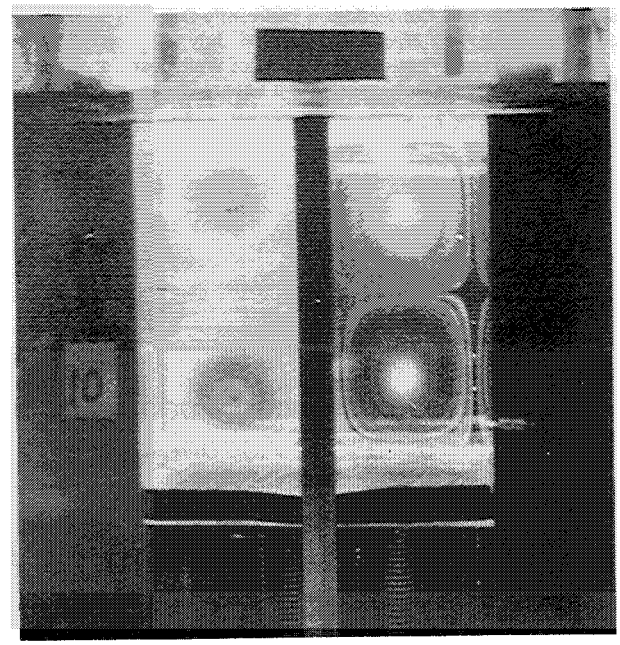

Fig. 13 Photograph of the flow pattern for $A = 1$, $H_2/L = 0.5$, $W/L = 0.1$, $Ra = 10^5$.

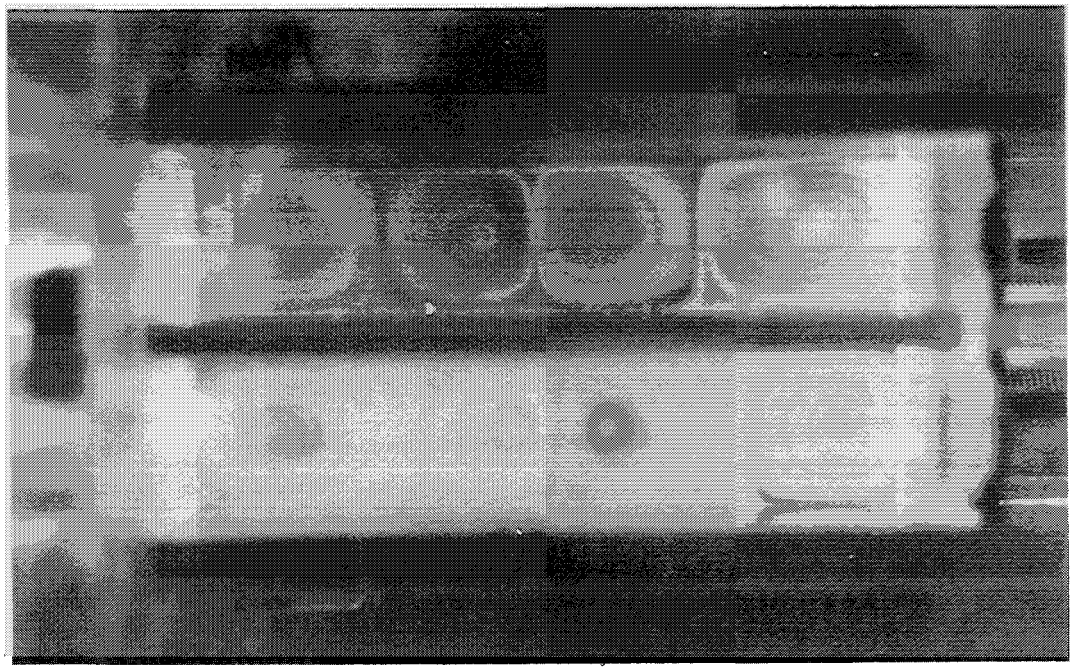

Fig. 14 Photograph of the flow pattern for $A = 2$, $H_2/L = 0.5$, $W/L = 0.1$, $Ra = 10^5$.

Acknowledgment

The authors would like to thank Mr. W. L. Tsai for his help in constructing the test section of the experiment.

References

[1]Ostrach, S., "Natural Convection in Enclosures," *Advances in Heat Transfers*, Vol. 8, 1972, pp. 161–227.

[2]Catton, I., "Natural Convection in Enclosures," *Proceedings of the 6th International Heat Transfer Conference*, Toronto, Canada, 1978, pp. 13–19.

[3]Koutsoheras, W. and Charters, W. W. S., "Natural Convection Phenomena in Inclined Cells with Finite Walls—A Numerical Solution," *Solar Energy*, Vol. 19, 1977, pp. 433–438.

[4]Viskanta, R. and Lankford, D. W., "Coupling of Heat Transfer Between Two Natural Convection Systems Separated By A Vertical Wall," *International Journal of Heat and Mass Transfer*, Vol. 24, July 1981, pp. 1171–1177.

[5]Kim, D. M. and Viskanta, R., "Study of the Effects of Wall Conductance on Natural Convection in Differently Oriented Square Cavities," *Journal of Fluid Mechanics*, Vol. 144, July 1984, pp. 153–176.

[6]Kim, D. M. and Viskanta, R., "Effect of Wall Heat Conduction on Natural Convection Heat Transfer in a Square Enclosure," *Journal of Heat Transfer*, Vol. 107, Feb. 1985, pp. 139–146.

[7]Samuels, M. R. and Churchill, S. W., "Stability of a Fluid in a Rectangular Region Heated from Below," *AIChE Journal*, Vol. 13, 1967, pp. 77–85.

[8]Blake, K. R., Bejan, A., and Poulikakos, D., "Natural Convection Near 4 °C in a Water Saturated Porous Layer Heated from Below," *International Journal of Heat and Mass Transfer*, Vol. 27, Dec. 1984, pp. 2355–2364.

[9]Catton, I. and Lienhard, V. J. H., "Thermal Stability of Two Fluid Layers Separated by Interlayer of Finite Thickness and Thermal Conductivity," *Journal of Heat Transfer*, Vol. 106, Aug. 1984, pp. 605–612.

[10]Lienhard, V. J. H. and Catton, I., "Heat Transfer Across a Two-Fluid-Layer Region," *Journal of Heat Transfer*, Vol. 108, Feb. 1985, pp. 98–205.

[11]Rubin, S. G. and Graves, R. A., "Viscous Flow Solution with a Cubic Spline Approximation," *Computers and Fluids*, Vol. 3, 1975, pp. 1–36.

[12]Rubin, S. G. and Khosla, P. K., "Higher-Order Numerical Solutions Using Cubic Splines," *AIAA Journal*, Vol. 14, 1976, pp. 851–858.

[13]Rubin, S. G. and Khosla, P. K., "Polynomial Interpolation Methods for Viscous Flow Calculations," *Journal of Computational Physics*, Vol. 24, July 1977, pp. 217–244.

[14]Wang, P. and Kahawita, R., "Numerical Integration of Partial Differential Equations Using Cubic Splines," *International Journal of Computer Mathematics*, Vol. 13, 1983, pp. 271–286.